IFSCC 2025 full paper (IFSCC2025-620)

Development of Bakuchiol Incorporated Nanoliposomes with Efficient Skin Penetration, High Stability and Safety for Anti-Aging Application

Siyuan Chen [1,2*], Xi Wang[1], Chensihui Xiong[1], Dan Luo[1], Jun Deng[2], Wei Liu [2*]

[1] Hangzhou Rebtech/Wuhan Best-Carrier Nanomedicine Research Institute, China;

[2] National Engineering Research Center for Nanomedicine, Huazhong University of Science and Technology, Wuhan, China

Email: maggie@hzrebtech.com, siyuan.chen@njtech.edu.cn

ABSTRACT

Although retinoids are attractive anti-aging ingredients, how to solve the instability and skin irritation issues remains a long-standing challenge. Bakuchiol, extracted from the seeds of *Psoralea corylifolia*, has gained popularity as an alternative to retinoids but shows higher tolerance and mildness. Bakuchiol could regulate retinoic acid receptors and downstream genes, promote collagen synthesis, anti-inflammation, soothe and reduce redness, and regulate aquaporins expression. However, low solubility and stability, poor skin permeability, and low bioavailability greatly affect its wide application.

In order to solve the abovementioned issues, we developed a bakuchiol-encapsulated nanoliposomes (BKC-NLPs) delivery system with supreme bioavailability and anti-aging effectiveness. To enhance the stability and solubility, bakuchiol was incorporated into nanoliposomes by a high-pressure homogenization method. By carefully optimizing the formulation, the added polyquaternium-51 did not affect the stability and cytotoxicity of BKC-NLPs, but can remarkably enhance the cellular uptake and skin permeation efficacy. The anti-aging effectiveness was systematically evaluated at the cellular level, 3D skin model and clinical trials.

In vitro skin permeation result showed that BKC-NLPs substantially promoted the skin penetration depth. Moreover, compared to free bakuchiol, BKC-NLPs significantly promoted cellular uptake and cell proliferation of human dermal fibroblasts cells, protected cells from oxidative damage, and decreased cell senescence. Furthermore, BKC-NLPs decreased MMP-1 and MMP-3 secretion, and exceedingly enhanced the collagen I and III secretion compared to the model group. Similia results were observed in the 3D skin model. In clinical trials, BKC-NLPs considerably decreased the wrinkle area, depth, and number in all the volunteers without causing any irritation as confirmed in the patch test. The safety was further validated in the human pacth test. All these data suggest the developed BKC-NLPs exhibited desirable skin penetration and anti-aging effectiveness with considerable stability and safety, which holds great potential for anti-aging application.

Keywords: Anti-aging, Barrier function, Bioavailability

---

1. Introduction

Bakuchiol, a naturally occurring meroterpene phenol extracted from the seeds of *Psoralea corylifolia*, has emerged as a promising retinoid alternative offering improved tolerance and mildness while maintaining comparable biological efficacy. It exhibits anti-inflammatory, anti-oxidant, anti-microbial, and anti-cancer properties[1]. In dermatological applications, bakuchiol has demonstrated significant potential in treating skin diseases, including psoriasis and atopic dermatitis, by modulating the immune response and reducing inflammation[2]. Additionally, its antioxidant activity helps protect skin cells from damage caused by free radicals, which are associated with skin aging and various skin disorders. Despite its promising biological effects, the clinical application of bakuchiol is severely hampered by its poor physicochemical properties, particularly its pronounced lipophilicity. Its limited aqueous solubility greatly decreases its formulation feasibility and bioavailability[3].

Liposomes, as nanoscale vesicles composed of phospholipid bilayers, have emerged as an attractive drug delivery system for enhancing the delivery efficiency of hydrophobic functional ingredients like bakuchiol. They offer a number of distinct advantages. Firstly, due to the unique bilayer structure, liposomes can simultaneously encapsulate hydrophilic agents in the aqueous core and lipophilic compounds within their lipid membrane. This property allows for the effective encapsulation of bakuchiol, protecting it from degradation and enhancing its solubility in the physiological environment[4-5]. Secondly, liposomes exhibited excellent biocompatibility and biodegradability. Since liposomes are composed of natural phospholipids which are similar to the components of cell membranes, the risks of immunogenicity and toxicity of liposomes are reduced. In addition, the surface-modification possibility allows liposomes to achieve specific targeting[6]. By conjugating ligands such as antibodies, peptides, or sugars onto the liposome surface, the liposomes can be directed to specific cells or tissues, thereby enhancing drug accumulation at pathological sites. Extensive preclinical evidence supports the efficacy of liposomal systems for hydrophobic drug delivery[7-8]. For example, liposomal formulations of doxorubicin (Doxil®) have shown improved pharmacokinetics and reduced cardiotoxicity compared to the free drug. In the case of other natural compounds with similar physicochemical properties to bakuchiol, liposomes have also been proven to enhance their solubility, stability, and bioavailability[9]. Furthermore, targeted delivery could enhance the accumulation in diseased tissues, such as inflamed skin or cancer cells, thereby increasing its therapeutic efficacy while minimizing side effects on healthy tissues[10]. However, systematic investigation of bakuchiol-loaded liposomes remains conspicuously absent from the literature.

In this study, we aim to develop a novel cationic liposome formulation loaded with bakuchiol (BKC-NLPs) to overcome the limitations of free-bakuchiol (Fig.1). The liposome preparation process will be optimized to achieve a high encapsulation efficiency and stable physical properties. Additionally, the in-vitro release characteristics of bakuchiol from the liposomes will be investigated to understand its controlled-release behavior. Moreover, in-vitro skin penetration properties and cell uptake behavior will be explored. Finally, the anti-aging efficacy of BKC-NLPs through in-vitro cell experiments, 3D skin models, and human clinical trials will be systematically studied to evaluate the biological activity of the bakuchiol-loaded liposomes. This BKC-NLPs will maximize bakuchiol's therapeutic potential and shed light on developing next-generation anti-aging skincare products.

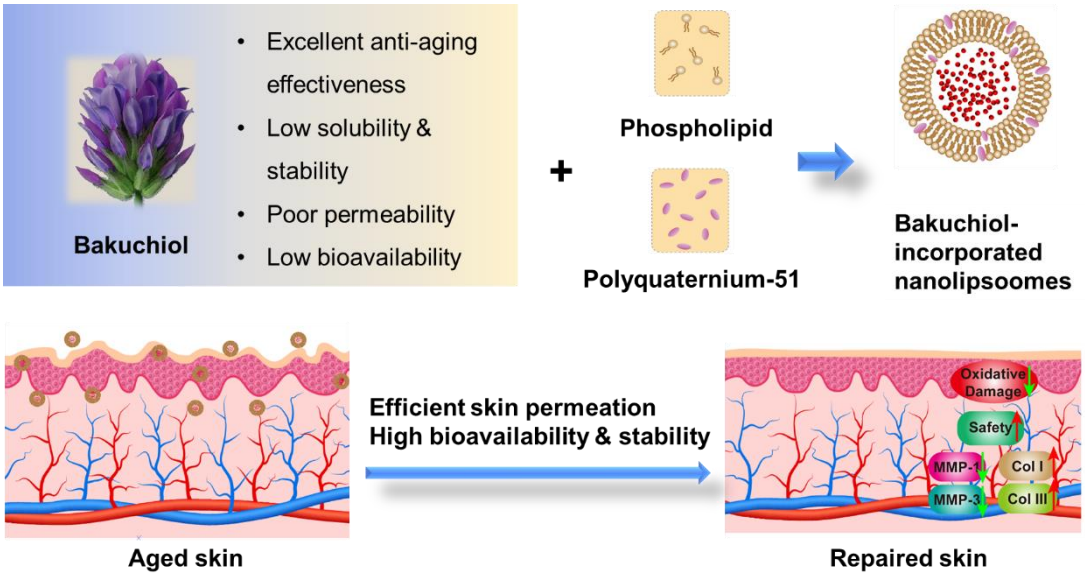

Fig.1. Schematic of bakuchiol-incorporated nanoliposomes for anti-aging application.

2. Materials and methods

2.1. Materials

Bakuchiol was purchased from Shaanxi Xintianyu Biotechnology Co., Ltd. (Shanxi, China). Phosphatidylcholine from soybean was obtained from Shanghai Taiwei Pharmaceutical Co., Ltd. (Shanghai, China). PEG-40 (CO40) was purchased from BASF Co., Ltd. (Ludwigshafen, Germany). TW-80, hydroxyacetophenone and phenylthiourea (PTC) were purchased from Aladdin Holdings Group Co., Ltd (Beijing, China). Polyglycerol-4 oleate was purchased from Sungrow Chemical Co., Ltd. (Tokyo, Japan). Dulbecco's modified Eagle's medium (DMEM), fetal bovine serum (FBS), phosphate-buffered saline (PBS, pH 7.4), penicillin, streptomycin, and trypsin-EDTA were obtained from Gibco (Gaithersburg, MD). Hydrogen peroxide (H_2O_2) was purchased from Sigma-Aldrich Co. (St. Louis, MO). The Reactive Oxygen Species (ROS), Matrix Metalloproteinases-1 (MMP-1), MMP-3, Collagen Type I (Col-I), Col-IV.

2.2. Cell Culture

HDF cells (SynthBio, Hefei, China) were all cultured in DMEM with 10 % FBS and 1 % penicillin/streptomycin. The cells were incubated in a humidified atmosphere of 5 % CO_2 at 37°C.

2.3. Preparation and characterization of BKC-NLPs

BKC-NLPs were prepared using a high-pressure homogenization technique. Briefly, 0.8% (w/w) polyquaternium-51, 10% (w/w) gLycerin, 12% (w/w) butylene glycol and 30.2% (w/w) water were mixed to produce phase A. 5% (w/w) lecithin, 5% (w/w) bakuchiol and 12% (w/w)1,5-pentanediol were mixed to produce phase B. 5 % (w/w) TCG, 10 % (w/w) CO40 and 10% (w/w) TW80 were mixed to produce phase C. The Phase A solution was stirred at 45°C until completely dissolved and transparent. Phase B was then stirred at 65 °C until homogeneous and transparent, after which it was cooled to 45 °C. Phase C was added to Phase B at 45 °C with continuous stirring, resulting in the formation of Phase D. Subsequently, Phase A was added to Phase D and stirred uniformly at 45°C, followed by filtration. The mixture was then homogenized using an AMH-3 microjet high-pressure homogenizer (Antos Nanotechnology, Suzhou, China) at 800 bar for three cycles. Finally, the BKC-NLPs sample was purified by ultrafiltration at 12,000 g for 15 minutes. RhoB-loaded NLPs (RhoB-NLPs) were prepared using the same procedure, except that RhoB was incorporated into Phase A as a replacement for the active ingredient.

The particle size and PDI were measured after 14 and 28 days. The drug loading efficiency (DLE) and encapsulation efficiency (EE) of the BKC-NLPs were measured by an ultrafiltration-centrifugation method. The content of BKC in the samples was analyzed using a BOCL 101 high performance liquid chromatography (HPLC) system (Shimadzu Instruments, Columbia, MD, UBKC) with a ChromCore AR C18 column (4.6 mm × 250 mm, 5.0 μm, Suzhou, China). acetonitrile : 0.1% - phosphoric acid water = 30:70 (v/v) was utilized as mobile phase for BKC detection, column temperature was set at 30°C, the UV detection wavelength was at 220 nm, injection volume was 20 μL, and flow rate was 1 mL/min. The DLE and EE of the BKC-NLPs were calculated using the following equations:

$$DLE(\%) = \frac{We}{Wm} \times 100$$

$$EE(\%) = \frac{We}{We+Wf} \times 100$$

In which We is the mass of the active ingredients encapsulated in the nanocarrier, Wm is the total mass of the nanocarrier, Wf is the mass of the free active ingredients not encapsulated in the nanocarrier.

The morphology of the BKC-NLPs was determined using transmission electron microscopy (TEM, HT7700, Hitachi, Tokyo, Japan). The BKC-NLPs were diluted for 400 times by deionized water, dropped on the copper grid, stained by 1% phosphomolybdic acid and air dried before observation by TEM.

2.4. Cellular Uptake Study of BKC-NLPs

HDF cells were seeded in 35-mm glass bottom dishes at a density of 2×10^5 cells per dish and incubated for 24 h, then treated with the Free-RhoB solution or RhoB-NLPs with the same RhoB concentration (2 μg/mL) and incubated for 4 h. Subsequently, the cells were washed three times with cold PBS and fixed with 4% paraformaldehyde in PBS for 15 min. After fixation, the cells were treated with DAPI solution (5 μg/mL) to label the nucleus, and imaged by a confocal laser scanning microscope with the excitation wavelength of 405 nm and 561 nm, respectively.

The uptake of the BKC-NLPs by HDF cells was further quantitatively analyzed by flow cytometry. HDF cells were seeded in 6-well-plates at a density of 3×10^5 cells per well separately and incubated for 24 h, then treated with the RhoB-NLPs or Free-RhoB solution with the same RhoB concentration (2 μg/mL) for 2 h or 4 h. After co-incubation, the culture medium was removed. The treated cells were washed with cold PBS, trypsinized, centrifuged and resuspended in 0.6 mL of cold PBS prior to flow cytometry analysis (FC500, Beckman Coulter, Fullerton, CA, USA) with the excitation wavelength of 561 nm.

2.5. Cell Proliferation Assay

HDF cells were seeded into 96-well plates at a density of 8×10^3 cells per well and cultured at 37 °C for 24 h. Each well was then supplemented with 100 μL of DMEM complete medium containing the BKC-NLPs at a BKC concentrations of 1.0, 2.0 and 4.0 μg/mL, as well as DMEM complete medium containing the Free-BKC (matching the active ingredient concentration of the BKC-NLPs). The 5-ethynyl-2′-deoxyuridine (EdU) assay was performed to assess the effect on cell proliferation. HDF cells were seeded in 15 mm glass-bottom dishes at a density of 2×10^5 cells per dish. After incubation for 24 h, the medium was substituted with BKC-NLPs and Free-BKC solution (matching the active ingredient concentration of the BKC-NLPs). The cells treated with DMEM only were served as the Control group. After incubation for 48 h, the cells were processed according to the manufacturer's instructions using a BeyoClick EdU Cell Proliferation Kit, and the nuclei were labeled with DAPI (2 μg/mL) for 10 min. The treated cells were observed using a CLSM. The excitation and emission wavelengths of Azide 488 (the fluorescence for labeling EdU) were 495 and 519 nm, respectively[11].

2.6. Detection of ROS Fluorescence Intensity

HDF cells were seeded into 24-well plates at a density of 4×10^4 cells/well, with 500 µL per well. After 24 h of culture, the supernatant was discarded. The model control group was supplemented with DMEM medium containing 0.6 mmol/L H_2O_2, while the other sample groups were supplemented with DMEM medium containing 0.6 mmol/L H_2O_2 and different concentrations of the test samples. A normal control group without H_2O_2 was also set up. After an additional 24 h of culture, DMEM containing 20 µM DCFH-DA was added and incubated for 20 minutes. The cells were washed three times with PBS, and the fluorescence intensity was observed under a fluorescence microscope. Cells were collected and the fluorescence intensity was analyzed using flow cytometry. A BKC concentration of 2.0 µg/mL of the BKC-NLPs and the Free-BKC was used as the experimental concentration.

2.7. Detection of anti-aging

HDF cells were seeded into 24-well cell culture plates at a density of 4×10^4 cells/well, with 500 µL per well, and cultured under conditions of 5 % CO_2 and 37 °C for 24 h. Next, the cultured cells were treated with BKC-NLPs or Free-BKC (matching the active ingredient concentration of the BKC-NLPs) in 0.8 mmol/L H_2O_2 at a BKC concentration of 1.0, 2.0 and 4.0 µg/mL for 24 h. The NC group received only 100 µL of DMEM complete medium. Each group had three replicates and was incubated in a CO_2 incubator for 24 h. The supernatant was then collected, and the levels of MMP-1, MMP-3, Col-I and Col-III were measured using ELISA kits.

2.8. 3D Skin Model Efficacy Study

The efficacy study was further carried out using commercially available epidermal tissue Exvivo® (Guangdong Biocell Biotechnology Co., Ltd., Dongwan, China), which is an in vitro reconstructed human epidermis (RHE) that is histologically similar to in vivo human epidermis. The Exvivo® models were removed from nutrient agar and equilibrated overnight in 6-well plates at 37 °C with 5% CO_2 and ~95% relative humidity. The model group, PC group, Free-BKC group, and BKC-NLPs group were stimulated with UVA (30 J/cm²) + UVB (50 mJ/cm²) for 24h. For the PC group, Exvivo® was treated with VC+VE (100µg/mL+7µg/mL) after UVA+UVB simulation. After incubation for 24 h, The models used for the assay were treated with 4% paraformaldehyde for fixation, and after 24 h fixation, immunofluorescence of the Collage-I and Collage-IV were detected. Images were taken and observed under the microscope, and 488nm was analyzed.

2.9. Human Skin Efficacy Study

Thirty-three adults between the ages of 30 and 55 years with significant facial wrinkles were selected as volunteers and randomly equalized into three groups. All subjects have provided informed consent. The 3% BKC-NLPs were homogenized into creams, the BKC-NLPs group was treated with one type of cream on the volunteers' faces once in the morning and once in the evening. In this experiment, all subjects were not allowed to use any skin-care ingredients on their faces, and the facial data of all subjects were collected and recorded by the Vplus Intelligent Analysis System on day 0 and day 28, respectively, and processed for analysis.

2.10. Statistical analysis

All results are shown as mean ± SD from at least three independent experiments. Statistical analysis was performed with one-way ANOVA. $P < 0.05$ was considered statistically significant.

3. Result

3.1. Characterization of BKC-NLPs

The particle size and stability affect the transdermal permeation behavior of NLPs, and therefore a series of characterization studies were conducted. The EE of the prepared BKC-NLPs was 94.2±0.6%, and the DLE was 4.61±0.18%. As shown in Fig.2, the developed BKC-

NLPs exhibit advantages such as uniform small particle size, high DLE and EE, and excellent stability, making them suitable for scalable industrial applications in transdermal delivery systems.

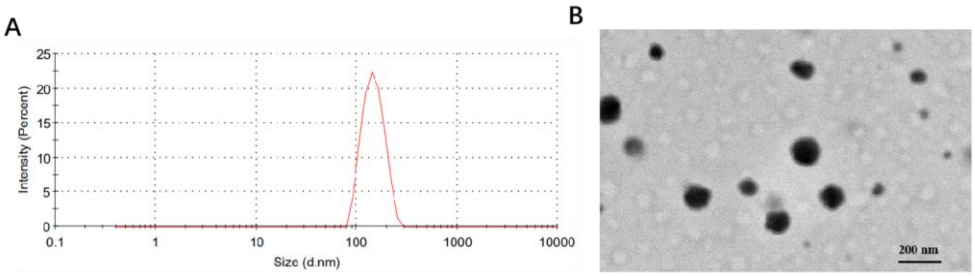

Fig.2. Characterization of BKC-NLPs. (A) Particle size of BKC-NLPs measured by DLS. (B) TEM images of BKC-NLPs. Scale bar: 200 nm.

3.2. Cellular Uptake Study

The cellular uptake behavior of HDF cells with RhoB-NLPs was observed using laser confocal microscopy. As shown in Fig.3a, after 2h of co-incubation with HDF cells, the fluorescence intensity within the HDF cells was relatively weak in the Free-RhoB group, while the red fluorescence was homogeneously distributed within the cells, indicating the RhoB-NLPs have already entered the cells. Furthermore, the fluorescence intensity was significantly stronger than that of Free-RhoB. After 4 h of incubation, the fluorescence intensity of the RhoB-NLPs was further enhanced. The experimental results indicate that, compared to Free-RhoB, the RhoB-NLPs were more effectively taken up by HDF cells, enabling the efficient delivery of the encapsulated active ingredients to target skin cells.

The cellular uptake was further quantified using flow cytometry. As seen in Fig.3b, after 2 and 4 h of incubation with HDF cells, the fluorescence intensity of RhoB-NLPs within the cells was significantly enhanced compared to Free-RhoB. This indicates that nanoliposomes are more readily taken up by HDF cells, enabling the efficient delivery of active ingredients to target skin cells and increasing both the uptake efficiency and intracellular accumulation of the active ingredients.

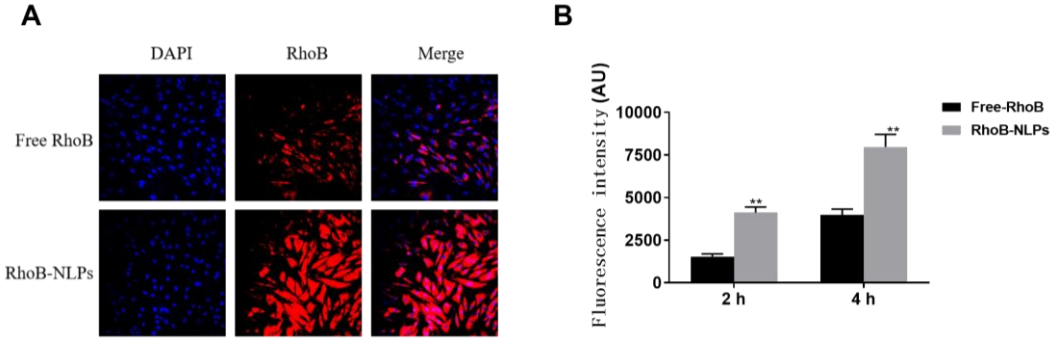

Fig.3. (A) Laser confocal microscopy observation of HDF Cell uptake behavior, and (B) flow cytometry detection of HDF cells uptake. $^{\#}P < 0.05$, $^{\#\#}P < 0.01$ vs NC, $^{\&}P < 0.05$， $^{\&\&}P < 0.01$ vs Free, Mean ± SD, n=3.

3.3. Results of Cell proliferation

The effect of different concentrations of Free-BKC and BKC-NLPs on the proliferation of HDF cells was shown in Fig.4a. Free-BKC and BKC-NLPs exhibited a significant increase in the cell viability of HDF cells. The cell viability increased gradually with the BKC concentration ranging from 1.0~4.0 μg/mL, exhibiting a dose-dependent effect. At a concentration of 4.0

μg/mL, the cell viability of HDF cells treated with BKC-NLPs was 11.86% higher than that of Free-BKC ($P < 0.01$). The cell proliferation was further assessed by EdU assay. As seen in Fig.4b, the EdU-positive cell rate of HDF cells treated with BKC-NLPs showed a substantial increase, with 94.9% higher than that of Free-BKC ($P < 0.01$), indicating that the BKC-NLPs promoted HDF cells proliferation more effectively than the same dose of Free-BKC.

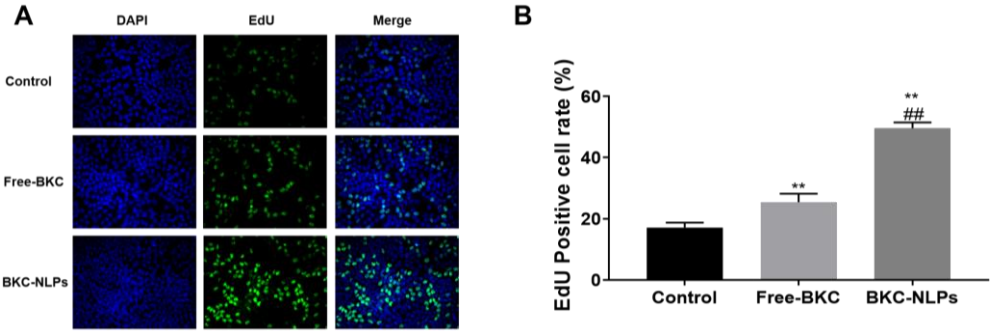

Fig.4. (A) Evaluation of positive HDF cells and (B) proliferation rates using the EdU assay, $^{\#}P < 0.05$, $^{\#\#}P < 0.01$ vs NC, $^{\&}P < 0.05$, $^{\&\&}P < 0.01$ vs Free, Mean ± SD, n=3.

3.4. Protection of HDF Cells from Oxidative Damage

ROS serves dual functions in the skin: it acts as a signaling molecule regulating repair and defense mechanisms at low levels, but when overproduced, it leads to oxidative stress, causing aging, inflammation, and skin damage[12]. Upon treatment with H_2O_2 in HDF cells, as shown in Fig.5, the fluorescence intensity within the cells increased, indicating that H_2O_2 induced oxidative damage. However, following the administration of Free-BKC and BKC-NLPs, the intracellular ROS fluorescence intensity was significantly reduced. Compared with Free-BKC, BKC-NLPs demonstrated superior efficacy in effectively countering oxidative stress-induced damage, with their effect markedly surpassing that of the same dose of Free-BKC.

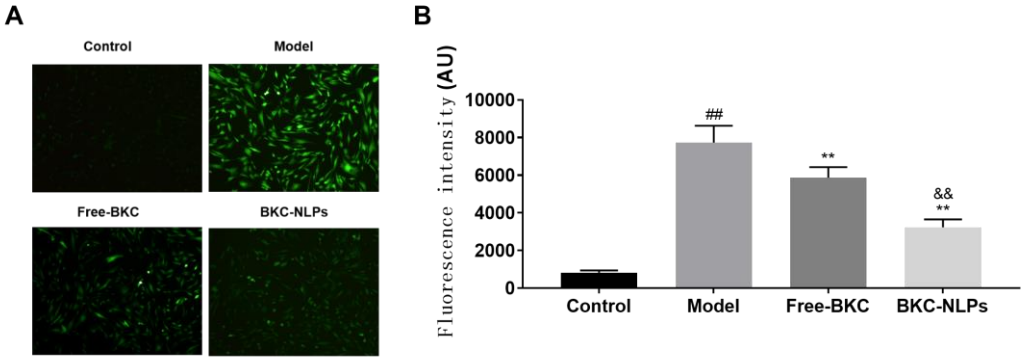

Fig.5. Effect of the BKC-NLPs protecting HDF cells from oxidative damage, $^{\#\#}P < 0.01$ vs Control; $^{**}P < 0.01$ vs MC; $^{\&\&}P < 0.01$ vs Free-BKC; Mean ± SD, n=3.

3.5. MMP and Colleague Secretion

MMP-1 and MMP-3 are enzymes that degrade extracellular matrix components, including Col-I and Col-III, which are key structural proteins maintaining skin elasticity and integrity. Excessive expression of MMP-1 and MMP-3 accelerates the breakdown of Col-I and Col-III, leading to weakened dermal structure, loss of elasticity, and visible signs of aging, such as wrinkles and sagging. Regulating MMP activity while promoting collagen synthesis is essential for preserving skin health and mitigating aging-related changes[13]-[14].

As shown in Fig.6, following H_2O_2-induced modeling, the expression levels of MMP-1 and MMP-3 significantly increased. This indicates enhanced activity of matrix metalloproteinases

(MMPs), which accelerate the degradation of the extracellular matrix (ECM). MMP-1 and MMP-3 are primarily responsible for collagen breakdown, particularly type I and type III collagen. Their upregulation further disrupts skin tissue structure, leading to reduced elasticity and impaired repair capacity. These results confirm the successful establishment of the cellular aging model.

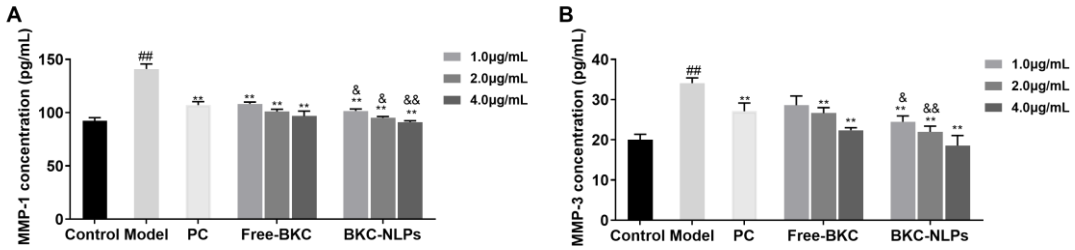

Fig.6. Effect of the BKC-NLPs on MMP-1 (A) and MMP-3(B), $^{\#\#}P < 0.01$ vs Control; $^{*}P < 0.05$,$^{**}P < 0.01$ vs Model; $^{\&}P < 0.05$, $^{\&\&}P < 0.01$ vs Free-BKC; Mean ± SD, n=3.

As shown in Fig.7, the expression levels of Col-I and Col-III were significantly reduced after H_2O_2-induced modeling. Col-I and Col-III are the major structural components of the skin's ECM, providing stability and elasticity. Their decline suggests an increased rate of collagen degradation, impaired tissue repair, and the onset of aging-related phenotypic changes such as wrinkles and skin laxity. The above results indicate that H_2O_2-induced oxidative stress markedly upregulates MMP expression while decreasing collagen levels, ultimately leading to ECM degradation, skin structural damage, and accelerated aging. Subsequent treatment with different doses of Free-BKC and BKC-NLPs reduced MMP-1 and MMP-3 activity while restoring Col-I and Col-III levels, demonstrating their ability to inhibit matrix metalloproteinase activity, limit collagen degradation, and exert anti-aging effects. Notably, BKC-NLPs exhibited superior efficacy compared to Free-BKC, underscoring the advantages of nanocarrier-based delivery systems for skin repair and anti-aging applications.

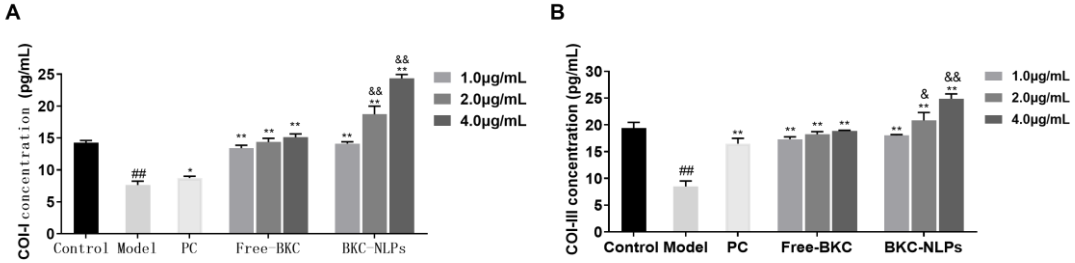

Fig.7. Effect of the BKC-NLPs on Col-I (A) and Col-III(B), $^{\#\#}P < 0.01$ vs Control; $^{*}P < 0.05$,$^{**}P < 0.01$ vs Model; $^{\&}P < 0.05$, $^{\&\&}P < 0.01$ vs Free-BKC; Mean ± SD, n=3.

3.6. 3D Skin Model Efficacy Study

Collagen I and Collagen IV are essential proteins in the skin, each serving distinct roles. Collagen I, primarily found in the dermis, provides structural strength and elasticity, enabling the skin to resist external damage and maintain its resilience. Collagen IV, on the other hand, is a critical component of the basement membrane, supporting cell adhesion, migration, and skin barrier integrity. Together, they ensure the skin's firmness, elasticity, and overall functionality, with their decline contributing to visible signs of aging, such as wrinkles and reduced skin strength[15-16]. As shown in Fig.8, exposure to UVA and UVB radiation led to a significant reduction in type I collagen levels, confirming the successful establishment of the skin aging model. Compared to the model group, fluorescence intensity measurements revealed that type

I collagen levels increased significantly by 168% in the Free-BKC group and 280% in the BKC-NLPs group.

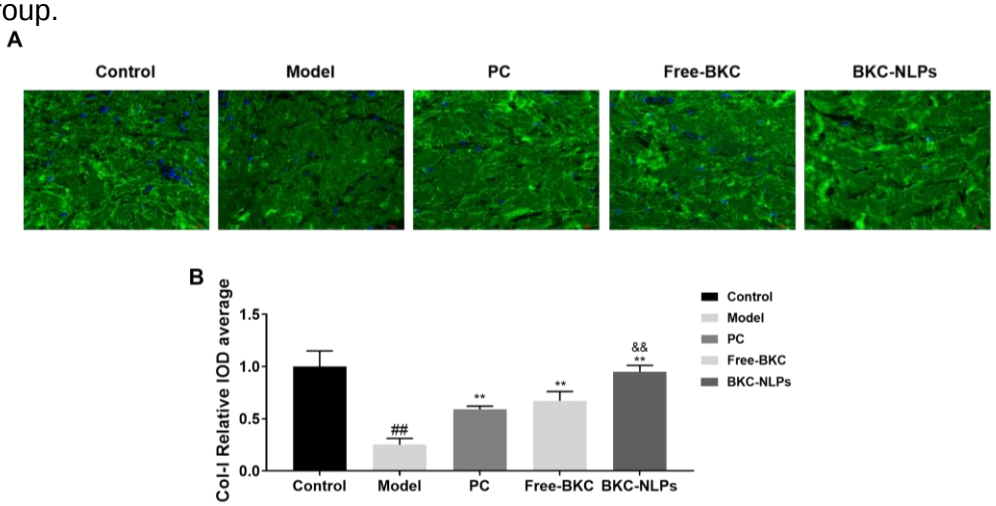

Fig.8. The anti-aging effect of BKC studied using the 3D skin models. Collagen I in the 3D skin model (A) and Collagen I was quantified by immunofluorescence microscopy (B). $^{\#}P < 0.05$, $^{\#\#}P < 0.01$ vs Control; $^{*}P < 0.05$, $^{**}P < 0.01$ vs Model; $^{\&}P < 0.05$, $^{\&\&}P < 0.01$ vs Free-BKC; Mean ± SD, n=3.

As shown in Fig.9, Collagen IV was also markedly reduced following UVA and UVB exposure. However, compared to the model group, fluorescence intensity analysis showed that type IV collagen levels were significantly enhanced by 147% in the Free-BKC group and 191% in the BKC-NLPs group. The results suggest that UVA and UVB exposure disrupts the structural integrity of the skin by degrading type I and type IV collagen, thereby accelerating the aging process. Both Free-BKC and BKC-NLPs effectively counteract collagen depletion, with BKC-NLPs exhibiting superior efficacy in restoring collagen levels. This indicates that BKC-NLPs enhance the anti-aging effects of BKC by providing a more efficient delivery system, offering potential applications in skin rejuvenation and photoprotection.

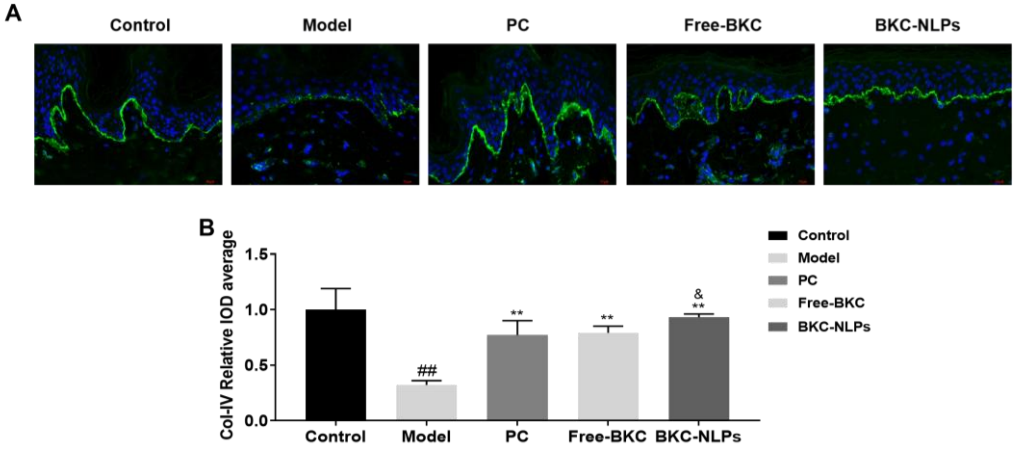

Fig.9. The anti-aging effect of BKC studied using the 3D skin models. (a) Collagen IV in the 3D skin model visualized by immunofluorescence microscopy. (b) Quantified Collagen IV. $^{\#}P < 0.05$, $^{\#\#}P < 0.01$ vs Control; $^{*}P < 0.05$, $^{**}P < 0.01$ vs Model; $^{\&}P < 0.05$, $^{\&\&}P < 0.01$ vs Free-BKC; Mean ± SD, n=3.

3.7. Human Skin Efficacy Study

The area of deep skin wrinkles and shallow skin wrinkles, and the number of wrinkles, are important parameters for evaluating the anti-aging effect of skincare products on facial skin. After 28 days of using the 3% BKC-NLPs Essence, the total area of deep facial skin wrinkles, the total area of shallow facial skin wrinkles, and the number of wrinkles of the volunteers were

significantly reduced, and the average area of heme was considerably improved. As seen in Fig.10, after 28 days of using the essence containing 3% BKC-NLPs, the total area of deep wrinkles, and the total area of shallow wrinkles of the volunteers' skin all improved. The total area of deep wrinkles decreased by 58.76% compared to the initial state, the total area of shallow wrinkles decreased by 45.31% compared to the initial state. These indicate that 3% BKC-NLPs exhibit pronounced anti-aging effects by notably reducing the number of crow's feet and the area of deep and shallow wrinkles within 28 days.

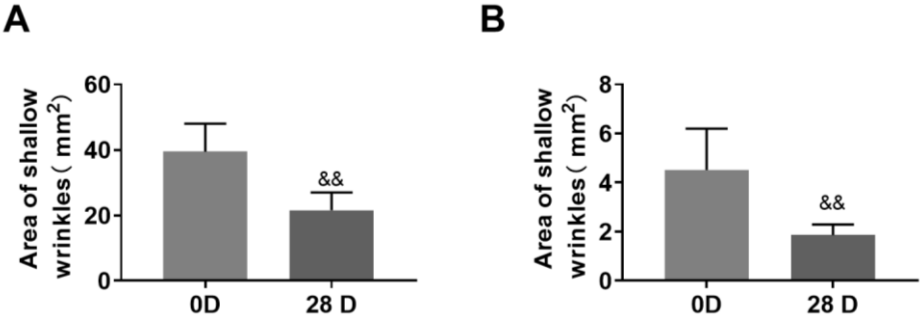

Fig.10. The anti-aging effect of BKC-NLPs studied using the human skin models. The area of (a) deep wrinkles and (b) shallow wrinkles. $^{\&}P < 0.05$，$^{\&\&}P < 0.01$ vs 0 D; Mean ± SD, n=30.

4. Conclusions

In this study, a bakuchiol-loaded cationic nanoliposomes delivery system was developed to improve the transdermal permeability and enhance the anti-aging effect of BKC. The prepared BKC-NLPs exhibited uniform nanoparticle size, good stability, high DL and EE, as well as improved transdermal permeability and enhanced cellular uptake. In addition, the systematic study at three levels (cellular, 3D skin models and human skin experiments) not only illustrated the anti-aging efficacy and mechanism of BKC to guide its application, but also proved that the BKC-NLPs can remarkably improve the anti-aging effect of BKC by enhancing the skin permeation of BKC. In conclusion, the developed BKC-NLPs with efficient skin penetration, high stability and safety is promising for anti-aging application.

References

[1] Nizam NN, Mahmud S, Ark SMA, et al. F1000Res. 2023,12:29.
[2] Puyana C, Chandan N, Tsoukas M. J Cosmet Dermatol. 2022,21(12):6636-6643.
[3] Mascarenhas-Melo, F., Ribeiro, M.M. Phytochem Rev, 2024, 23:1377-1413.
[4] Farooq, M.A., Trevaskis, N.L. 2023,40:245-263.
[5] Mascarenhas-Melo, F., Ribeiro, M.M., Kahkesh, K.H. et al. Phytochem Rev. 2024,23:13 77-1413.
[6] Akbarzadeh, A., Rezaei-Sadabady, R., Davaran, S. et al. Nanoscale Res Lett. 2013, 8: 102.
[7] Almeida, B., Nag, O.K., Rogers, K.E., et al. Molecules. 2020, 25:5672.
[8] Nsairat H, Khater D, Sayed U, et al. Heliyon. 2022,8(5):e09394.
[9] Sushil Rana, Deep Narayan Sharma, Sahil Chandel, et al. World J Pharmaceu life sci. 2025, 11(3):191-198.
[10] Sonju, J.J., Dahal, A., Jois, S.D. et al. Peptide Therapeutics. 2022,47:203-235.
[11] Zhang S, Zhou H, Chen X, et al. ACS Appl Mater Interfaces. 2024,16(13):15701-1571 7.
[12] Hong, Y., Boiti, A., Vallone, D., et al. Antioxidants. 2024, 13:312.
[13] Loo YC, Hu HC, Yu SY, et al. Phytomedicine. 2023,110:154643.
[14] Cui B, Wang Y, Jin J, et al. Oxid Med Cell Longev. 2022,2022:6037303.
[15] Tan, I.J., Silver, F.H, et al. J Theoreti Bio. 2025,4:3-29.
[16] Zhang W, Zheng Z, Wang T, et al. ACS Appl Mater Interfaces. 2024,16(42):56744-56 761.